

ORIGINAL

ARTICLE



Fast serotonin voltammetry as a versatile tool for mapping dynamic tissue architecture: I. Responses at carbon fibers describe local tissue physiology

Aya Abdalla*¹, Alyssa West*¹, Yunju Jin†, Rachel A. Saylor*, Beidi Qiang‡, Edsel Peña§, David J. Linden†, H. Frederik Nijhout¶, Michael C. Reed**, Janet Best†† and Parastoo Hashemi* 

*Department of Chemistry and Biochemistry, University of South Carolina, Columbia, South Carolina, USA

†Solomon H. Snyder Department of Neuroscience, The Johns Hopkins University School of Medicine, Baltimore, Maryland, USA

‡Department of Mathematics and Statistics, Southern Illinois University Edwardsville, Edwardsville, Illinois, USA

§Department of Statistics, University of South Carolina, Columbia, South Carolina, USA

¶Department of Biology, Duke University, Durham, North Carolina, USA

**Department of Mathematics, Duke University, Durham, North Carolina, USA

††Department of Mathematics, The Ohio State University, Columbus, Ohio, USA

Abstract

It is important to monitor serotonin neurochemistry in the context of brain disorders. Specifically, a better understanding of biophysical alterations and associated biochemical functionality within subregions of the brain will enable better understanding of diseases such as depression. Fast voltammetric tools at carbon fiber microelectrodes provide an opportunity to make direct evoked and ambient serotonin measurements *in vivo* in mice. In this study, we characterize novel stimulation and measurement circuitries for serotonin analyses in brain regions relevant to psychiatric disease. Evoked and ambient serotonin in these brain areas, the CA2 region of the hippocampus and the medial prefrontal cortex, are compared to ambient and evoked serotonin in the

substantia nigra pars reticulata, an area well established previously for serotonin measurements with fast voltammetry. Stimulation of a common axonal location evoked serotonin in all three brain regions. Differences are observed in the serotonin release and reuptake profiles between these three brain areas which we hypothesize to arise from tissue physiology heterogeneity around the carbon fiber microelectrodes. We validate this hypothesis mathematically and *via* confocal imaging. We thereby show that fast voltammetric methods can provide accurate information about local physiology and highlight implications for chemical mapping.

Keywords: confocal microscopy, FSCV, hippocampus, medial forebrain bundle, prefrontal cortex, substantia nigra. *J. Neurochem.* (2019) <https://doi.org/10.1111/jnc.14854>

Received January 18, 2019; revised manuscript received February 27, 2019, June 27, 2019; accepted July 12, 2019.

Address correspondence and reprint requests to Parastoo Hashemi, 631 Sumter St, Columbia, SC, 29208, USA. E-mail: hashemi@mail-box.sc.edu

¹These authors contributed equally to this work.

Abbreviations used: CFM, carbon fiber microelectrode; FSCV, fast-scan cyclic voltammetry; FSCAV, fast-scan controlled adsorption voltammetry; SNr, substantia nigra pars reticulata; PFC, prefrontal cortex; mPFC, medial prefrontal cortex; MFB, medial forebrain bundle; CV, cyclic voltammogram; SEM, standard error of the mean; RRID, Research Resource Identifiers.

Neuromodulators, such as serotonin, are thought to regulate the brain's major excitatory and inhibitory processes. As such, subtle alterations in the function of these modulators are thought to underlie the phenotypes of many disorders of the brain (Owens and Nemeroff 1994; Abi-Dargham *et al.* 1997; Volkow and Fowler 2000; Oades 2008; Muller *et al.* 2016). To better understand the functional importance of messengers like serotonin in the brain, analytical measurements of neurotransmitters is a thriving and rapidly evolving field (Meunier *et al.* 2017; Johnson *et al.* 2018; Shen *et al.* 2018). To this end, we have thus far focused on pioneering *in vivo* measurements of evoked and ambient serotonin using fast-scan cyclic voltammetry (FSCV) and fast-scan controlled adsorption voltammetry (FSCAV) at carbon fiber microelectrodes (CFMs) (Hashemi *et al.* 2009; Abdalla *et al.* 2017).

Quantitative chemical measurements of brain serotonin *in vivo* are highly challenging because of very low extracellular concentrations (Parsons and Justice 1993). An additional difficulty for electroanalytical measurements is that serotonin and serotonin metabolites are detrimental to electrode stability because of polymer filming (Jackson *et al.* 1995). In our initial efforts to develop an FSCV tool for serotonin measurements, we chose to make measurements in the substantia nigra, pars reticulata (SNr) because this region contains the most dense innervation by serotonin axons in the brain (Palkovits *et al.* 1974). When it comes to interest in serotonin's actions in the brain, however, there is much focus on psychiatric, cognitive, and developmental disorders (Owens and Nemeroff 1994; Abi-Dargham *et al.* 1997; Volkow and Fowler 2000; Oades 2008; Muller *et al.* 2016) which implicate brain regions other than the SNr. These brain regions include the hippocampus (Gyorfı *et al.* 2017), amygdala (Schumann *et al.* 2011), hypothalamus (Nestler *et al.* 2002), and prefrontal cortex (PFC) (Jin *et al.* 2016). Our own research interests incline us toward the hippocampus and medial prefrontal cortex (mPFC). Biophysical alterations are seen in these regions during disease. For example, volume changes in the hippocampus and the prefrontal cortex have been associated with depression (Bremner *et al.* 2000; Bremner *et al.* 2002; Frodl *et al.* 2006; Rigucci *et al.* 2010). It is very important to address the chemical functionality associated with such biophysical changes. We have performed pilot studies in these and other brain areas (Srejjic *et al.* 2016; Abdalla *et al.* 2017; West *et al.* 2018), here we present a formal characterization of the voltammetry stimulation and measurement circuits for serotonin in the CA2 region of the hippocampus and the mPFC, compared with the SNr.

Serotonin is shown to be evoked in the CA2 region of the hippocampus, the mPFC and the SNr *via* a common electrical stimulation of the medial forebrain bundle (MFB). Comparison of the evoked and ambient serotonin chemistry in these three regions reveals significant

differences which we postulate to arise from differences in tissue physiology local to the CFM, specifically in the characteristics of serotonin reuptake *via* different monoamine transporters. The chemical signals are modeled mathematically according to our previously established models of serotonin transmission which accounts for Uptake 1 [Serotonin transporter (SERT) mediated] and Uptake 2 [Dopamine transporter (DAT), norepinephrine transporter (NET), and organic cation transporter (OCT) mediated] (Wood *et al.* 2014) and single versus dual-evoked events (West *et al.* 2018). Our modeling also, independently, hypothesizes differences in how serotonin is reuptaken *via* Uptake 1 and 2, while bringing forth additional hypotheses about the strength of input to the three locales and autoreceptor contribution. Our models' predictions are subsequently verified with confocal imaging of axons and stimulation parameter experiments.

We thereby show that FSCV and FSCAV are multifaceted tools that provide information on the proteins directly around the CFM and tell us about the strength of the input circuit. This combination of techniques presents an innovative approach for chemical brain mapping which has future implications for chemically defining the functionality of local circuitry during health and disease. A better understanding of the circuits within specific brain regions will ultimately allow for improved drug targeting for disease treatment.

Materials and methods

Study design and exclusion criteria

Previously collected sample data (see Data S1) informed upon values necessary to determine statistical difference between two serotonin signals. These data were input into a power analysis according to literature standards (Charan and Kantharia 2013). The following formula to calculate sample size between two groups with a quantitative endpoint was used:

$$n = 2 \times SD^2 \times (Z^\alpha + Z^\beta) / d^2$$

The pooled standard deviation from the sample data was found to be 1.06, and the effect size 1.96, resulting in a calculated Cohen's *d* of 1.85 (Cohen 1988). The Z^α term used was 1.96 according to a 95% confidence interval and the Z^β term was 0.842 according to the 80% power assumed. This power analysis resulted in a $n = 5.25$, which was rounded to five. Finally, the sample size was corrected to account for loss of animals because of death or exclusion criteria (Charan and Kantharia 2013). We began with 141 animals to accommodate this adjustment and still achieve sufficient power. The percent of animals expected to die because of urethane anesthesia, based on empirical observations from our own laboratory, was about 38% (54 of 141 animals). This number appears high, though research has shown that many studies severely under-report unexpected death from anesthesia (Uhlıg *et al.* 2015). Urethane is a terminal anesthetic and the dose is difficult to adjust. However, the fact that our experiments require long periods of stable anesthesia,

combined with the non-survival nature of our experiments makes urethane an ideal choice for our purposes. Of the remaining 87 animals, 34 were excluded for because of exclusion criteria fully detailed below, leaving 53 animals that were included in the data analysis (16 in the SNr, 16 in the CA2 and 21 in the mPFC). No randomization was used to determine which mice would be used for the measurement in each region. (Fig. 1).

For all FSCV experiments, the CV of the evoked signal was compared to well-established serotonin cyclic voltammograms (CVs) *in vivo* and *in vitro* and mice in which the CVs did not contain the characteristic serotonin redox peaks or included interference by dopamine were excluded. For FSCAV experiments, a stimulated serotonin response was collected prior to the start of FSCAV and the same aforementioned test was performed. Data which contained a stimulation artifact resulting from the stimulation electrode touching the skull that masked, delayed, or minimized the serotonin response (stimulation glitch) were excluded. Electrodes that displayed drift or instability during file collection, as a result of damage during insertion, were excluded. While stereotaxic technique was utilized for this study, individual variation between mice oftentimes limits the control we have over the exact position of the working electrode. We confirmed placement of the electrode in our target region in two ways, first during surgery, if the cyclic voltammogram is characteristic for serotonin and second, post-surgery histology confirmed if the electrode was in the target region. Signals not collected in the target regions were excluded from the study.

Carbon-fiber microelectrodes

CFM's were constructed through the aspiration of a single T-650 carbon fiber (7 μm ; Goodfellow, Coraopolis, PA, USA) through a cylindrical glass capillary (internal diameter: 0.4 mm, external diameter: 0.6 mm, Product # 624500; A-M Systems, Carlsborg, WA, USA). This capillary was then placed in a vertical pipette

puller (Narishige Group, Setagaya-Ku, Tokyo, Japan) to make a carbon-glass seal by gravity. The protruding carbon fiber was then cut to 150 μm in length. Subsequently, a solution of Nafion (LQ-1105-US-25, 5% by weight Nafion; Ion Power, New Castle, DE, USA) was electrodeposited, as previously described, onto the exposed carbon fiber (Hashemi *et al.* 2009). The CFM was then dried for 10 min at 70°C.

Animal surgery

C57BL/6J (Research Resource Identifiers, RRID: IMSR_JAX:000664) male mice, 6–12 weeks old and between 20 and 30 g, were procured from Jackson Laboratories (Bar Harbor, ME, USA). The study was originally started with 141 mice. Mice were offered food and water *ad libitum* and housed in 12 h light/dark cycles. The Guide for the Care and Use of Laboratory Animals, as accepted by the Institutional Animal Care and Use Committees of the University of South Carolina (Institution Approval # A3049-01), was followed in all animal care and procedures. A urethane solution was produced (25% (w/v)) by dissolving urethane (Product # U2500; Sigma Aldrich Co., St. Louis, MO, USA) in sterile saline (0.9% NaCl solution, NDC 0409-4888-20; Hospira, Lake Forest, IL, USA). The anesthetic urethane, was administered intraperitoneally (i.p.) at a volume of 7 μL per 1 g mouse weight, followed by stereotaxic surgeries (Model 962; David Kopf Instruments, Tujunga, CA, USA) during the light cycle. To maintain the ideal mouse body temperature of 37°C, a heating pad from Braintree Scientific was utilized. For stereotaxic coordinates of MFB [AP: -1.58, ML: +1.0, DV: -4.8 to -5.0], SNr [AP: -3.28, ML: +1.40, DV: -4.21 to -5.0] CA2 [AP: -2.9, ML: +3.35, DV: -2.5 to -3.0], and mPFC [AP: +1.7, ML: +0.2, DV: -2.0 to -3.0], bregma was used as a reference from Franklin and Paxinos (2008). In order to access the MFB, CA2, SNr, and mPFC holes were drilled in line with the above stereotaxic coordinates. No randomization method was used to assign mice for measurements in a specific region. For

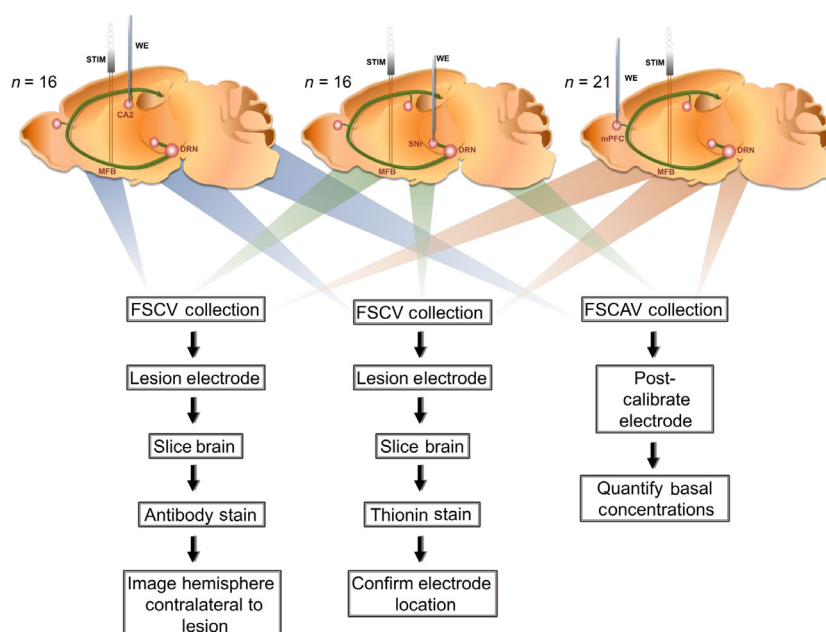


Fig. 1 In each of the three brain regions [CA2, substantia nigra pars reticulata (SNr), medial prefrontal cortex (mPFC)] serotonin measurements were taken using either fast-scan cyclic voltammetry (FSCV) or fast-scan controlled adsorption voltammetry (FSCAV). The three main methods, outlined here, led to the collection of evoked control (SNr: $n = 5$, CA2: $n = 5$, mPFC: $n = 10$), evoked stimulation parameter experiments (SNr: $n = 5$, CA2: $n = 5$, mPFC: $n = 5$), and basal (SNr: $n = 5$, CA2: $n = 5$, mPFC: $n = 5$) serotonin measurements, and staining of serotonin axons (SNr: $n = 1$, CA2: $n = 1$, mPFC: $n = 1$) in each of the three regions of interest. (n = number of animals).

stimulation, a stainless-steel electrode (diameter 0.2 mm, MS303/2-A/SPC; Plastics One, Roanoke, VA, USA) was inserted into the MFB. For measurements, the Nafion-coated CFM was then inserted into either the CA2, SNr, or the mPFC. The reference electrode is made of a silver wire (diameter: 0.010 in, 787000; A-M Systems, Sequim, WA, USA), which was electroplated with chloride through immersion of in hydrochloric acid for 30 s (0.1 M, 4 V vs. tungsten). This is then placed into the contralateral hemisphere of the CFM placement.

Data collection

FSCV and FSCAV were both performed through instrumentation and software (WCCV 3.05) developed by Knowmad Technologies LLC (Tucson, AZ, USA) (available upon request). FSCV was performed by applying the “Jackson” waveform (Jackson *et al.* 1995). Measurements were collected every 10 min with a 30–60 s file. Five seconds into the file, a stimulation was applied (60 Hz biphasic 360 μ A, 120 pulse stimulation, 2 ms per phase) through employing a linear constant current stimulus isolator (NL800A Neurolog; Digitimer Ltd., Hertfordshire, UK) to elicit serotonin response. This stimulation was varied slightly, one parameter at a time, for the stimulation parameter experiments. FSCAV was applied through a CMOS precision analog switch, ADG419 (Analog Devices, Norwood, MA, USA), which is used to control the application of the computer-generated “Jackson” waveform to the CFM. The logic was software-controlled to either apply a series of ramps (0.2 V to 1.0 V to -0.1 V to 0.2 V, scan rate = 1000 V/s) every 10 ms (100 Hz) or apply a constant potential of 0.2 V to the CFM for a specified controlled adsorption period (10 s) (Abdalla *et al.* 2017).

Data analysis

Signals collected from FSCV and FSCAV were processed using custom software (*vide supra*) using LabVIEW 2009 (available upon request). The processing used includes signal deconvolution, filtering and smoothing. For FSCAV, the cyclic voltammogram (CV) at the 3rd scan (following the controlled adsorption period) was extracted to integrate the serotonin oxidation peak approximately between 0.4 V and 0.85 V. The charge value found, in pC, was plotted versus [serotonin] to generate calibration curves that were then used to calculate *in vivo* values which were specific to each electrode (Abdalla *et al.* 2017). No blinding was necessary for the purpose of the experiments presented herein.

Statistical analysis

Post hoc validation of sample size

A sample size of five mice for each of the three groups was utilized. This choice of sample size was initially estimated by previous studies (see Study Design) as the data necessary for proper sample size calculation was not yet collected. Following collection of experimental data, this sample size was reevaluated based on power considerations. We assumed that two-sample *t*-tests applied at 5% level of significance and an 80% power with a Cohen's *d* of 2.0 (associated with an effect size of 2 from experimental data), when the common standard deviation is 1.0. Note that based on the obtained sample data, the pooled standard deviation was found to be

1.06, which is close to 1.0. Based on the sample size formula, the appropriate sample size to use is thus $n = 3.92$, rounded to a sample size of four for each group. Taking into consideration that the assumed common standard deviation of 1.0 may have been too liberal (in light of the sample standard deviation of 1.06), a sample size of five per group appears acceptable for determining statistical differences.

Basal level analysis

In vitro calibrations related charge with the concentration, as explained previously (Abdalla *et al.* 2017). We compared the basal responses for the three regions (CA2, SNr, mPFC; five animals for each region), where the basal value was measured every minute for 60 min. Hence, a repeated-measures two-factor model was fitted, with the factors being the region and time. To accommodate the repeated-measures feature, random effects were included in the model, as well as the possible interaction effects between region and time. The model developed is presented here:

$$Y(I, j, t) = M + A(i) + B(t) + C(i, t) + V(I, j) + E(I, j, t).$$

Where $i = 1, 2, 3$ represents the region; $j = 1, 2, \dots, 5$, represents the animal number (within the group), and $t = 0, 1, 2, \dots, 60$, represents the time. M is a common mean; the $A(i)$'s are the effects of the region levels; the $B(t)$'s are the effects of the time levels; the $C(I, t)$'s are the interaction effects; $V(i, j)$ is a random term (which is normally distributed) to account for the repeated measurements over time; and $E(I, j, t)$'s are the error terms (which are also normally distributed and independent of the $V(I, j)$'s).

A test of the null hypotheses that the $B(t)$'s and $C(I, t)$'s are all zeros based on the repeated-measures analysis of deviance, implemented through the R Statistical Package, resulted in not being able to reject these null hypotheses, hence both the interaction effect and the time effect were not significant. The p -value for testing for no interaction effects was 0.8539, whereas the p -value for testing that there is no time effect is 0.8249.

Because the time and region*time effects were not significant, we therefore combined the concentration over the 60 min for each of the animals in each group by obtaining their sample means. These sample mean values were then used to compare whether there were differences between the three regions; this analysis was performed using a one-way analysis of variance. By analyzing the sample means of the observations over time, we were able to eliminate dependencies over time among the observations. This analysis of variance showed that at least two of the regions are indeed different statistically with a p -value of 0.00000756 (ANOVA).

To determine which regions are different, we performed pairwise *t*-tests with the Welch–Satterthwaite's degrees-of-freedom approximation to allow for unequal variances, and we implemented a multiple testing correction, using the Holm procedure. We concluded that CA2 and mPFC regions are not statistically different (adjusted $p = 0.23$), whereas the SNr and CA2 are different (adjusted $p = 0.000012$), and the SNr and mPFC are also different (adjusted $p = 0.000043$). A summary of the statistics from these group means are provided in the table below, which includes 95% confidence interval for the group means.

Region	Sample size	Mean (mean of the sample means)	SD (standard deviation)	ME (margin of error)	95% CI for the group mean response
SNr	5	39.706	4.391	5.452	34.254–45.158
CA2	5	72.822	7.170	8.903	63.919–81.725
mPFC	5	67.565	7.636	9.481	58.084–77.046

Depletion analysis

Repeated stimulations were employed to determine if serotonin release could be depleted in each of the three regions over time. Maximum serotonin release for each animal in each group was measured in response to stimulations every minute for 20 min. The main goal was to compare the maximum amplitude during the first stimulation ($t = 1$) with those at later times to see whether serotonin release was depleted in response to repeated stimulations. Because this is a repeated-measures experiment, for any fixed time t (taking values from 2, 3, ..., 20), we took the differences in the level at time t and at time 1 for each of the animals within each group. Using these differences, we then performed a one-sample t -test to test the null hypothesis that the population mean difference is zero versus less than zero (indicating a decrease from time 1 to time t). We performed this procedure for each of the time values t , yielding a t -test statistic value and a p -value. Since we performed multiple tests (19), we applied the Benjamini–Hochberg (BH) false discovery rate (FDR) multiplicity correction. The results are as follows, based on the BH-adjusted p -values:

For the CA2 dataset, we concluded that the maximum amplitude at $t = 20$ is significantly lower than at $t = 1$, with BH-adjusted p -value of 0.0325. This is the only time point for which we concluded significance based on the BH-adjusted p -values. It should be noted that some of the unadjusted p -values arising from these t -tests were less than .05, however, the necessity of the multiplicity adjustments increased these values. It is possible that with more animals, statistical significance could be achieved. Another way to globally test if the serotonin level was decreasing over time is *via* an analysis of covariance with the covariate being the serotonin level at $t = 1$. This analysis of covariance yielded an estimate of the regression coefficient associated with time of -0.4542 (p -value = 0.00048) and with estimate of the coefficient of determination of $R^2 = 59.66\%$. The sign of the estimated regression coefficient (negative), indicates that the serotonin level decreases over time from $t = 1$.

For the SNr dataset, we did not find any significant differences between $t = 1$ and any of the other time points, even before the BH adjustment for multiplicity. An analysis of covariance also did not show a significant decrease.

For the mPFC dataset, prior to the BH multiplicity adjustments, there were p -values that were less than 0.05. After employing the BH-adjustments the analysis concluded no significant differences between the $t = 1$ and later time values. An analysis of covariance did not show a significant difference in the serotonin level over time.

Modeling

We use the mathematical model that we previously presented (Wood *et al.* 2014):

$$\frac{d[S(t)]}{dt} = R(t)(1 - A(t)) - \alpha \frac{V_{\max 1}[S(t)]}{K_{m1} + [S(t)]} - \beta \frac{V_{\max 2}[S(t)]}{K_{m2} + [S(t)]}$$

$S(t)$ is the concentration of serotonin in the extracellular space, $R(t)$ is the firing rate of the serotonin neuron that rises briefly after stimulation, and $A(t)$ represents the strength of the autoreceptor effect. The first negative term represents reuptake by SERTs with $V_{\max 1} = 19.25$ nM/hr and $K_{m1} = 5$ nM. The second term represents Uptake 2 (DATs, NETs, and OCTs) with $V_{\max 2} = 780$ nM/hr and $K_{m2} = 170$ nM. Uptake 2 operates only above the steady-state concentration of serotonin. α and β give the balance between Uptake 1 and Uptake 2. For details and discussion, see Wood *et al.* (2014). To model the double peak in the mPFC we use the extended model presented in West *et al.* (2018) that allows diffusion of serotonin from regions with only Uptake 1 to regions that have both Uptake 1 and Uptake 2.

Histology

In order to confirm the spatial placement of the CFM *in vivo*, a small lesion was created at the end of the FSCV experiment, by applying a constant potential at the CFM (~ 10 V for 1 min). Subsequently, the mice were sacrificed via cervical dislocation followed by decapitation, and the brain was removed from the skull and stored in 4% paraformaldehyde in PBS solution. At least 2 days prior to sectioning, the brain was transferred into a 30% sucrose solution, until it was saturated with the medium. The brain was then flash-frozen, sectioned into 30 μ m slices mounted onto frosted glass slides, and stained with 0.2% thionin. The slices were then photographed with a camera attached to an optical microscope.

Immunohistochemistry

Slc6a4-EGFP male mice (RRID: MMRRC_030692-UCD), 6- to 12-week old, were anesthetized with urethane (25% dissolved in 0.9% NaCl solution, Hospira, Lake Forest, IL) administered intraperitoneally (i.p.) at a volume of 7 μ L per 1 g mouse weight. Mice were then perfused intracardially with phosphate-buffered saline (PBS) followed by 4% paraformaldehyde in PBS at 4°C. The entire brain was removed and fixed in 4% paraformaldehyde for 3 h at room temperature ($\sim 23^\circ\text{C}$) and then cryoprotected in 15% sucrose in PBS overnight at 4°C, followed by a switch to 30% sucrose on the next day and continuing overnight. Sections of the mouse brain (40 μ m thick) were prepared using a microtome and were washed with PBS and then blocked with 5% normal goat serum and 0.3% Triton X-100 in PBS for 2 h at room temperature ($\sim 23^\circ\text{C}$). The sections were incubated in primary antibody diluted in blocking buffer, overnight at 4°C. The primary antibodies used were chicken anti-GFP (1 : 5000; Aves Labs, Davis, CA, USA, #GFP-1010, RRID: AB_2307313), guinea pig anti-SERT (1 : 1000; Frontier Institute, Hokkaido, Japan, #HTT-GP-Af1400), rabbit anti-TH (1 : 1000; Millipore Corporation, Burlington, MA, USA, #AB152), and mouse anti-NeuN (1 : 500; Millipore, Burlington, MA, USA, #MAB377, RRID: AB_2298772). The sections were then washed with PBS and incubated in the secondary antibody in a blocking buffer for 2 h at room temperature ($\sim 23^\circ\text{C}$). The secondary antibodies used were Alexa Fluor 488-labeled goat

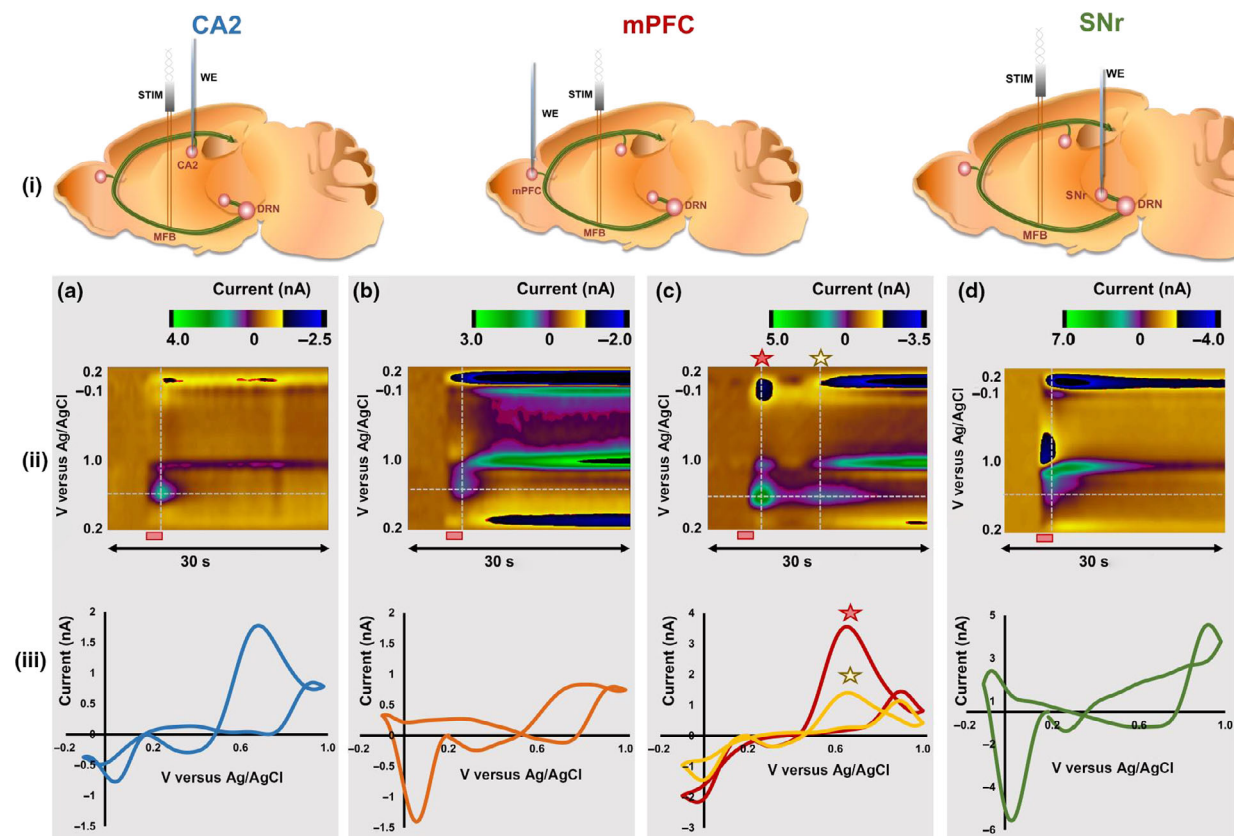


Fig. 2 (i) Representation of a sagittal section of a mouse brain. WE shows the position of the working electrode and STIM shows the stimulating electrode. Green track represents the serotonergic axons that originate in the raphe nucleus and traverse the medial forebrain bundle to innervate different brain regions. (ii) Representative fast-scan cyclic voltammetry color plots of the CA2 (a) ($n = 5$), the medial prefrontal cortex (mPFC) (b) ($n = 5$) and (c) ($n = 5$), and the substantia nigra pars reticulata (SNr) (d)

($n = 5$). The red bar below the color plots denotes the stimulation period (2 s) (iii) Cyclic voltammograms extracted from the vertical dashed lines in a(ii), b(ii), c(ii), and d(ii) with current on the y-axis and voltage versus Ag/AgCl on the x-axis. Red and yellow stars on c(ii) denote the two successive oxidation events seen in the mPFC. Cyclic voltammograms extracted at both these positions are seen in c(iii), marked with their respective stars. ($n =$ number of animals).

anti-chicken (1 : 1000; Life Technologies, Carlsbad, CA, USA, #A11039), Cy3-labeled goat anti-guinea pig (1 : 800; Jackson Immuno-Research, West Grove, PA, USA, #106-165-003), Cy3-labeled goat anti-rabbit (1 : 800; Jackson ImmunoResearch Laboratories, West Grove, PA, USA, #111-165-003), and Cy5-labeled goat anti-mouse (1 : 200; Jackson ImmunoResearch Laboratories, West Grove, PA, USA, #115-175-146). Then, the sections were mounted on slides, and images were acquired using a single-photon confocal microscope (Zeiss, Oberkochen, Germany). Maximum projection images of 10 z-planes 1 micron apart were analyzed using NIH ImageJ (<https://imagej.nih.gov/ij/>), and % pixel intensity of EGFP signal above threshold was measured as an index of SERT innervation.

Results

Serotonin is evoked via a common MFB stimulation in three distinct brain regions

Stimulation of the MFB at one location evokes serotonin in the CA2 region of the hippocampus, the mPFC and the SNr. Figure 2 displays representative examples of color plots and

CVs collected in each of these three brain areas upon stimulation. In Panel (i) are illustrations of the positions of the stimulating and working electrode in sagittal sections of the mouse brain. Panel (ii) shows representative 30 s color plots enveloping the 5 s before and 25 s after the stimulation. Interpretation of color plots is explained in detail elsewhere (Michael *et al.* 1999), briefly voltage is on the y-axis, time on the x-axis, and current illustrated in false color. Panel (iii) shows CVs extracted from the vertical dashed lines on the color plots with the oxidation peak of serotonin at approximately 0.7 V.

In contrast to the CA2 and SNr where a single serotonin release and uptake event is evoked upon stimulation, in the mPFC we often also observe a dual peak, the origins of which we've recently described (West *et al.* 2018). Two representative examples of mPFC signals are illustrated in Fig. 2(c).

To study whether there is physiological relevant information in these traces, we carry out a comparison of how

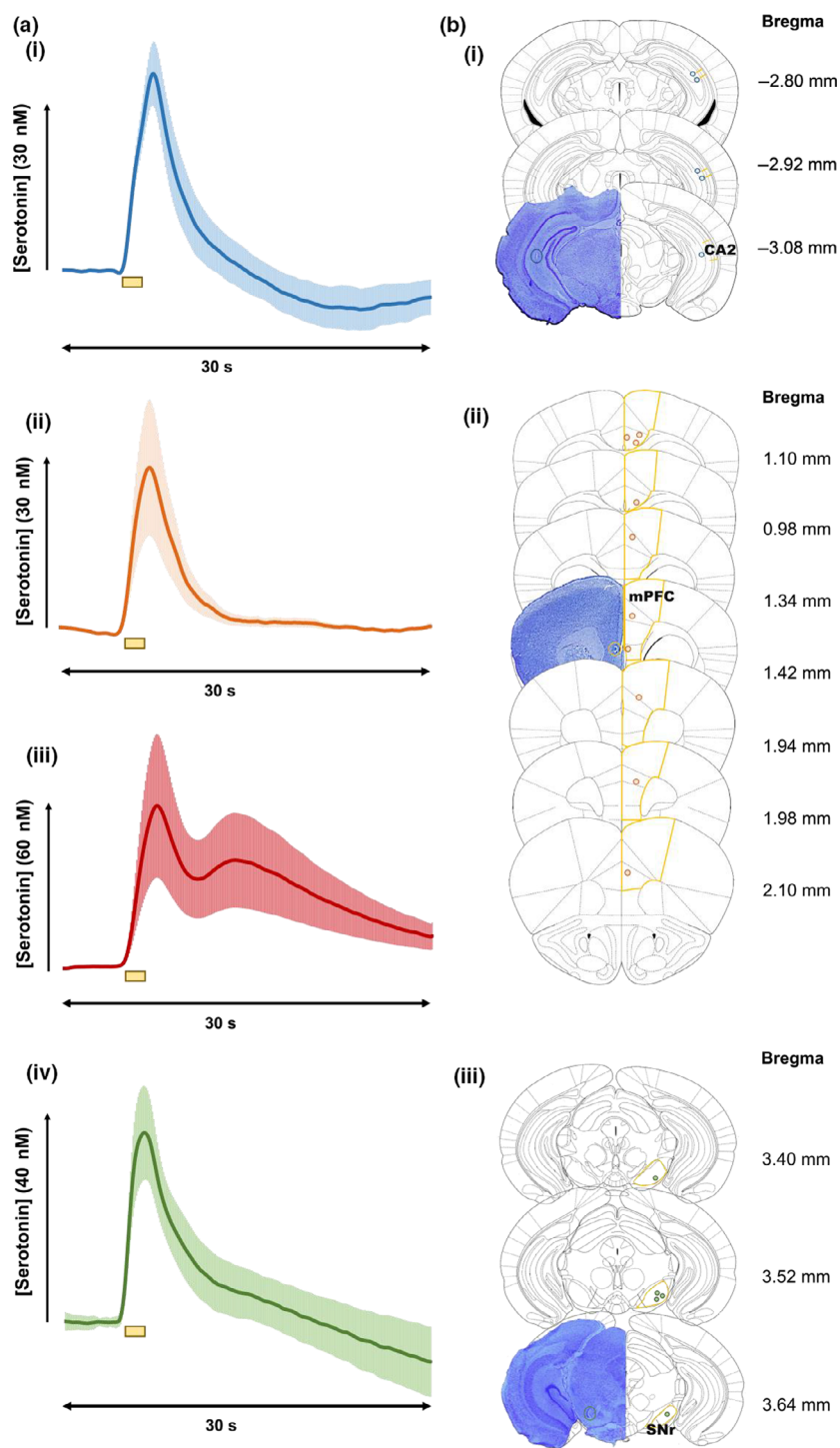


Fig. 3 (a) Averaged [Serotonin] – time profiles ($n = 5 \pm \text{SEM}$) (i) CA2, (ii) Medial prefrontal cortex (mPFC) single peak response, and (iii) mPFC double peak response, and (iv) Substantia nigra pars reticulata (SNr). Yellow bars beneath the plot denote the stimulation period (2 s). (b) Thionin-stained representative brains displayed on the left with a colored circle denoting the actual placement of the carbon fiber microelectrodes (CFM). On the right, yellow lines represent the outlines of the (i) CA2 (ii) mPFC, and (iii) SNr regions. Blue, orange, and green circles denote the placement of the CFM in each individual mouse, for the CA2 ($n = 5$), the SNr ($n = 5$), and the mPFC ($n = 10$), respectively. Coordinates with respect to Bregma are shown to the right of each coronal slice. Region-specific coordinates are explained in the methods section. ($n =$ number of animals).

serotonin concentration changes over the file collection time. Serotonin concentration [serotonin] versus time traces are extracted at the position of the peak oxidation current and averaged between five animals per region. Figure 3 shows the averaged serotonin time courses per region [$n = 5$, \pm standard error of the mean (SEM)]. The responses are confirmed to be in the target region *via* lesioning the tissue

adjacent to the CFM after the experiment. A representative stained slice from each region, along with the location of the CFM, for each experiment performed can be found in Panel (b) of Fig. 3. The decay of these traces indicates the transporters responsible for removing serotonin from the extracellular space. A fast decay is a result of Uptake 2 (DATs, NETs, and OCTs), a slow decay results from Uptake

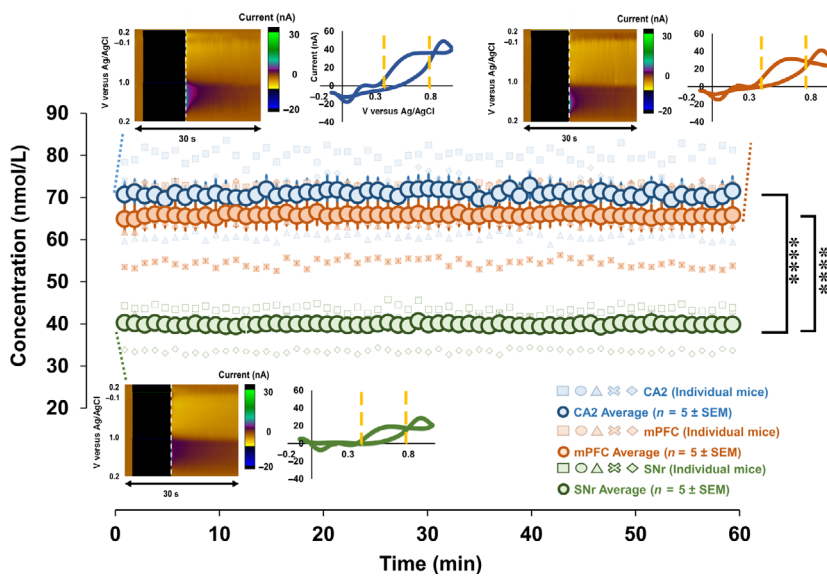


Fig. 4 Blue, orange and green circles represent the weighted averaged response ($n = 5$ mice each region \pm SEM), and faint blue, orange, and green markers represent individual mice responses. Files were collected for 60 mins to obtain a baseline reading. Representative fast-scan controlled adsorption voltammetry color plots and cyclic voltammograms (CVs) (extracted from vertical dashed lines) are inset, on top left for the CA2, top right for the medial prefrontal cortex (mPFC), and at the bottom for substantia nigra pars reticulata (SNr). Yellow lines on the CV denote the limits of integration. **** $p < 0.0001$.

1 (SERTs), and a trace which has both fast and slow decay is a hybrid response and results from a combination of the two uptakes. Serotonin release in the CA2 appears primarily mediated by Uptake 2. The mPFC serotonin responses, as we previously characterized (West *et al.* 2018), involve clearance by both Uptake 1 and 2 transporters, which are linked inextricably to the two release domains. Serotonin released in the first domain, observed as a single peak, is reuptaken by Uptake 2 mechanisms, whereas serotonin in the second domain is solely reuptaken by Uptake 1 processes. This was verified pharmacologically using escitalopram. Domain 2 is only readily observed when measurements occur in layers 5–6 of the mPFC and is more sparsely innervated, resulting in a second peak because of the longer diffusion time to reach the electrode surface. In the SNr, serotonin seems to be reuptaken *via* a hybrid of Uptake 1 and 2.

These data lead us to formulate a hypothesis that the chemical decay profile after stimulation offered by the CFM is indicative of the ratio of SERT (Uptake 1) : non-SERT (Uptake 2), specifically that serotonin in the SNr is cleared by a higher Uptake 1 : Uptake 2 ratio when compared with the other two regions. To strengthen this hypothesis, we perform ambient serotonin measurements with FSCAV in the three brain areas, shown in Fig. 4.

Serotonin basal levels differ based on brain region

To measure ambient serotonin levels in each of three brain localities, a new method, FSCAV is applied (Abdalla *et al.* 2017). First MFB stimulation is employed in mice to verify the presence of serotonin with FSCV. FSCAV is then performed on the same CFM for 60 mins to obtain a baseline reading of ambient serotonin concentrations. The dark blue, green, and orange circles on the central trace of Fig. 4 represent the weighted average response ($n = 5 \pm$ SEM) in

the three regions. Individual mice traces are displayed by faint markers, of similar color, on the same plot. Representative *in vivo* color plots, along with CVs extracted from the 3rd scan (vertical dashed line), post-controlled adsorption period, can be seen on Fig. 4. All CVs demonstrate the characteristic redox serotonin peaks, thus confirming the identity of the signal measured. To convert this signal to serotonin concentration in the three regions, we use a chemometric approach, to take into account the variability between the CFMs used, along with the *in vivo* variability. This approach was explained in detail previously (Abdalla *et al.* 2017). Using 5 mice for each region, the average ambient serotonin level in the CA2 is 72.82 ± 3.21 nM ($n = 5$ mice, weighted average \pm standard error), the mPFC is 67.57 ± 3.42 nM ($n = 5$ mice, weighted average \pm standard error), whereas the level in the SNr is 39.71 ± 1.96 nM ($n = 5$ mice, weighted average \pm standard error). A pairwise *t*-test confirms statistically significant differences in the basal levels between the CA2 and SNr ($p = 0.000012$), and the mPFC and SNr ($p = 0.000043$). While the CA2 and mPFC are not statistically different from one another ($p = 0.23$). See the analysis reported earlier.

Mathematical modeling of evoked release

The ambient measurements support the idea that serotonin release in the SNr is reuptaken with a higher Uptake 1 : Uptake 2 ratio than in the CA2 or mPFC. Here, we analyze the experimental curves with previously established models and allow the model to generate an independent hypothesis to explain the experimental data. The model utilizes the Uptake 1, Uptake 2, autoreceptor, and two domain theories to determine the best parameters for fitting the experimental data presented here (Wood *et al.* 2014; West *et al.* 2018). Figure 5 shows the mean experimental

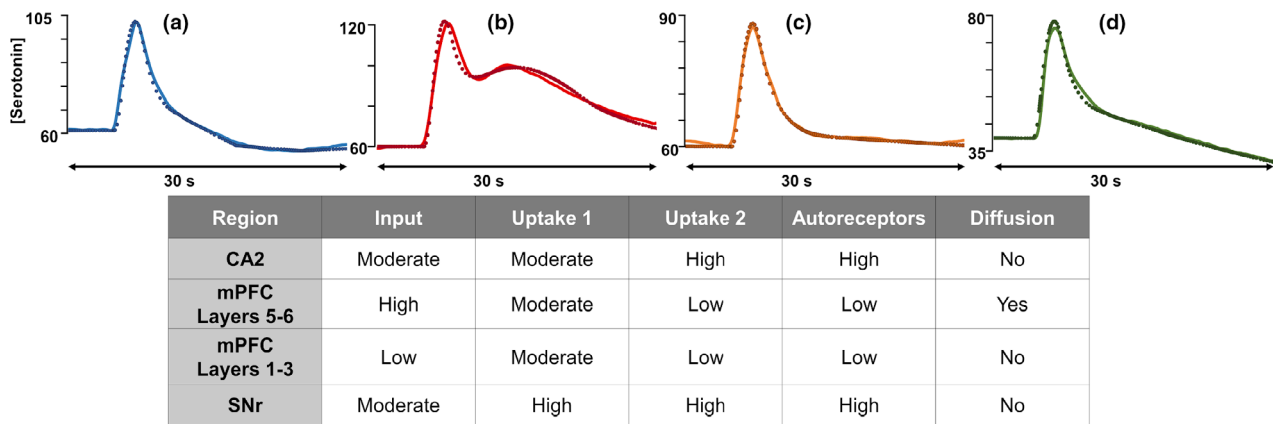


Fig. 5 The [Serotonin] versus time plots display the experimental data (solid) and model curves (dotted) for each region: CA2 (a), medial prefrontal cortex (mPFC) layers 5–6 (b), mPFC layers 1–3 (c), and

the substantia nigra pars reticulata (SNr) (d). The table below outlines the parameters used to generate the model curves for each region.

curves for the CA2, mPFC, and the SNr (solid are experimental and dotted are models).

This analysis gives us an opportunity to compare the three areas by comparing the models' parameters that were optimized to fit each curve. We allow ourselves to vary the strength of the input ($R(t)$), the strength of the autoreceptor effect ($A(t)$), and the strengths of Uptake 1 and Uptake 2 (α and β). And, to obtain the double peak in the mPFC, we allow diffusion from a region with only Uptake 1 to a region with both Uptake 1 and 2 (see West *et al.* 2018). The table in Fig. 5 shows the qualitative differences in the parameters for different regions.

The results from the modeling are as follows:

- (i) Diffusion is needed to explain the double peaks seen in the PFC.
- (ii) There is higher contribution of Uptake 1 in the SNr than in the other regions.
- (iii) The autoreceptor effect is strong in the SNr and CA2 but weak in the mPFC.
- (iv) The input strength to regions of the mPFC is more variable than to the SNr and CA2.

The model's results bring forth two additional hypotheses, (ii) and (iv), that we are able to test below.

Imaging axonal density in three brain regions

To test the hypothesis brought forth by the model's 2nd result (higher contribution of Uptake 1 in SNr) we employ a single photon imaging approach, whereby axons are imaged in brain slices of adult serotonin transporter-EGFP BAC transgenic mice (Gong *et al.* 2003). The imaging locations are chosen to correspond to the regions of our voltammetric measurements as ascertained with the histological analysis in Fig. 3.

Figure 6 shows exemplar confocal images taken from the prefrontal cortex, hippocampus CA2, and substantia nigra

pars reticulata (SNr) from serotonin transporter-EGFP BAC transgenic mice.

To compare the degree of innervation between the regions, the percent pixels were calculated across the same number of focal planes for each region. The results, seen in Table 1, illustrate a higher degree of serotonin axon innervation in the SNr compared to the two regions (innervation depends on layer and subregion of CA2 and mPFC).

Axonal reaction to electrical stimulation

To test the hypothesis brought forth by the model's 4th result (input strength to mPFC is more variable than other two regions) we perform a stimulation parameter study. Figure 7 (top panel) shows the maximum evoked concentration of serotonin after systematic variation in stimulation conditions frequency, amplitude, and pulse width. These data show that the axons react in a similar manner to stimulation since increased terminal serotonin accompanies increased stimulation intensity, frequency, and pulse width. It is only the mPFC response that does not substantially plateau during any of the stimulation paradigms, whereas the CA2 and SNr responses plateau during one or more of the experiments (CA2 and SNr during amplitude and SNr during frequency). The plateau of the curves are confirmed utilizing the first derivative of each point with respect to the previous one. In one or more of the parameter studies, the first derivative of the CA2 and SNr data fall below zero, indicating that the slope is plateauing. A depletion study, where serotonin release is stimulated once a minute over a 20 min period, is shown in Fig. 7 (bottom panel). Here, when accounting for multiplicity, serotonin release in the CA2, but in the SNr or mPFC, shows significant depletion over 20 stimulations (see Statistical Analysis section).

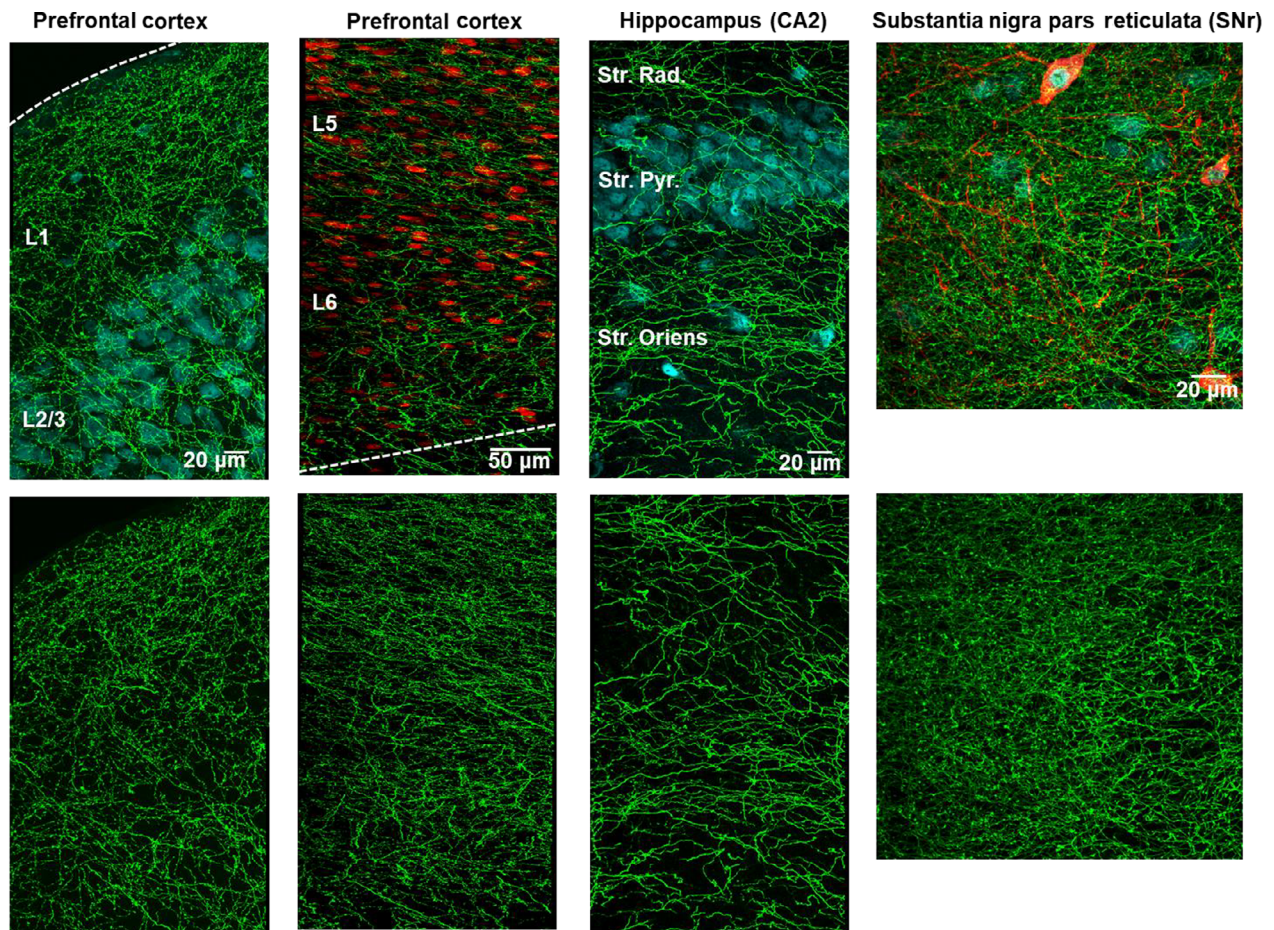


Fig. 6 Immunohistochemistry for GFP in serotonin transporter-EGFP BAC transgenic mice reveals serotonin axon density across brain regions ($n = 1$ mouse per region). Top panels: The SERT signal is shown in green with NeuN in cyan in all regions except the prefrontal cortex layer 5 and 6 where NeuN is shown in red. Layers 1–6 are all clearly defined in the prefrontal cortex and the stratum radiatum (Str. Rad.), stratum pyramidale (Str. Pyr.), and the stratum oriens are

labeled in the hippocampus. In the substantia nigra pars reticulata (SNr), the red immunofluorescence is signal from an antibody directed against tyrosine hydroxylase, a marker of dopamine neurons. The top panels show single photon confocal micrographs of axonal innervation in the three brain areas. The bottom panels show the green channel alone to allow for the clear comparison of serotonin axon density.

Discussion

Expanding serotonin voltammetry beyond the SNr

In vivo FSCV measurements are largely limited to dopamine. Serotonin is significantly more problematic to electroanalyze *in vivo* for two reasons. First, during the oxidative scan, serotonin and similarly structured metabolites form unstable intermediary species that rapidly restabilize by forming polymers (Jackson *et al.* 1995). Unfortunately, as this happens on the electrode surface, serotonin films are created which poison the electrode. Second, extracellular serotonin levels are low, being subject to a thorough level of regulation, likely because of serotonin's well-established neurotoxic effects (Lane and Baldwin 1997). The former issue was largely resolved *ex vivo* via a combination of kinetic and physical modifications to the electrode and

detection scheme (Jackson *et al.* 1995; Hashemi *et al.* 2009). The latter challenge was addressed by targeting an *in vivo* brain region with the highest density of serotonergic innervation, the SNr (Palkovits *et al.* 1974), under the rationale that the extracellular serotonin levels in that region should be high. Paradoxically, for reasons described below, we now know that extracellular serotonin levels in the SNr are not as high as in the other regions we studied.

Recent interest in serotonin dynamics is largely for its roles in affective, cognitive, and developmental disorders (Owens and Nemeroff 1994; Abi-Dargham *et al.* 1997; Volkow and Fowler 2000; Oades 2008; Muller *et al.* 2016). To investigate these diseases, brain regions other than the SNr are thought to play important roles. For example, the hippocampus is heavily implicated in emotion and memory, and as such is often the focus of depression studies (Gyorfi *et al.* 2017).

Similarly, the amygdala, nucleus accumbens, and hypothalamus are investigated for their roles in depression and anxiety (Nestler *et al.* 2002; Gina *et al.*, 2012). The prefrontal cortex plays a role in controlling cognition, motor function, affective, and social behaviors (Kolb *et al.* 2012). The region also has a prolonged development period which means particular susceptibility to influence from exposure to environmental risk factors (Muhammad *et al.* 2012). As such, the PFC is often associated with and considered in the study of developmental disorders. General and our own interest in these regions shifted our efforts toward serotonin FSCV measurements in the CA2 region of the hippocampus and the mPFC.

It is not trivial to simply apply our current FSCV approach to serotonin measurements in new brain regions. This is primarily because of interference from other transmitters,

Table 1 The degree of serotonin axon innervation was calculated as the percent of GFP-immunopositive pixels above threshold for each layer/ subregion within the three target regions

Region	Subregion/layer	% Pixels
CA2	Oriens	16.3
	Pyramidale	10.6
	Radiatum	15.9
SN	Pars Reticulata	27.4
mPFC	L 1	19.7
	L 2/3	14.6
	L 5	17.4
	L 6	14.9

mPFC, medial prefrontal cortex.

metabolites and ions, and the heterogeneity of serotonin release sites within each region. Nonetheless, we optimized stereotaxic coordinates that yield serotonin FSCV signals in the CA2 region of the hippocampus, the mPFC and the SNr, in separate animals, through electrical stimulation of a common MFB site. Figure 2 shows three representative color plots and corresponding CVs for signals obtained in these regions. It is important to mention that the examples we choose in this figure are highly representative of the signals we obtain in each region. The color plots and CVs are different in these regions, with unique additional features, speaking to the different interferences and microenvironment around the CFM. One such unique feature is the ‘switching’ peaks of each region that occur when analytes adsorb to the electrode surface and change the capacitive current that occurs as a function of the electrical bilayer on the electrode surface. This capacitive or charging current is normally subtracted out, however, when analytes adsorb and change the current, a signal is manifested at the positive and negative switching potentials. It is not easily possible to identify which analytes are responsible for the switching peaks, but the switching peaks are different in each region depending on the microenvironment. The characteristic serotonin oxidation peak is at around 0.7 V and we use this to quantify serotonin. Upon initial inspection of the CV, this peak can occasionally be difficult to observe because of the large switching peaks. However, upon closer inspection, including subtracting out the large switching peaks, the characteristic serotonin oxidation peak is observed.

The mPFC is an intrinsically unique brain region in the context of evoked serotonin responses where two types of signals are routinely observed. In contrast to the CA2 and

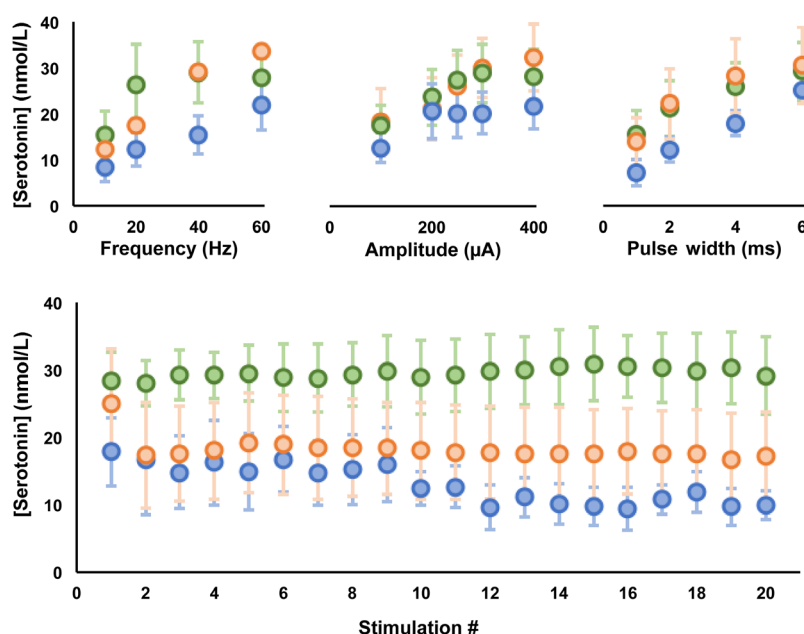


Fig. 7 Top panel – averaged serotonin responses ($n = 5$, \pm SEM), CA2 (blue), medial prefrontal cortex (mPFC) (orange) and in the substantia nigra pars reticulata (SNr) (green) with variation in the stimulation frequency (top left), stimulation amplitude (middle), and stimulation pulse width (top right). Bottom panel – average serotonin response ($n = 5$, \pm SEM) to a stimulation train for 20 mins at 60 Hz, 4 ms pulse width, and 360 μ A in the SNr (green), CA2 (blue), and mPFC (orange). (n = number of animals).

SNr where a single serotonin release and uptake event is evoked upon stimulation, in the mPFC we often also observe a dual peak. We recently characterized mPFC responses and showed that the dual response was because of stimulation of two distinct axonal bundles that traverse the MFB with diffusion to the electrode surface resulting in the two distinct peaks. Each domain was also found to have a specific reuptake mechanisms (Uptake 1 or Uptake 2) which was verified pharmacologically using escitalopram (West *et al.* 2018).

These data thus confirm serotonin release in three regions *via* stimulation of the same MFB coordinate. This common stimulation site is significant because it will enable future, simultaneous measurements of serotonin in multiple brain localities in one animal.

We perceive that the most striking feature of these responses is the difference in reuptake profiles. To better provide a visual comparison, in Fig. 8, these responses are normalized such that the maximum amplitude in each case is at the level of the horizontal blue dotted line. In Wood *et al.* 2014, we modeled the uptake of serotonin in the SNr *via* two mechanisms, Uptake 1 and 2, first coined by Sol Snyder in the 1970s (Shaskan and Snyder 1970). Uptake 1 is reuptake by the serotonin transporters (SERTs) at high affinity and low efficiency. We observe the Uptake 1 mechanism as a single, slow decay curve (approx. 12–15 s). Uptake 2 transpires because of the activity of non-serotonin (non-SERT) transporters, that uptake serotonin with high efficiency, but with low capacity. Uptake 2 generates a decay curve with a single slope that reaches baseline quickly (around 5 s). When there is a combination of SERTs and non-SERTs, the result is a hybrid signal, with a curve that decays quickly for a few seconds, followed by a slow decay until it reaches baseline, resulting in decay with two different slopes (Wood *et al.* 2014).

While the latter portions of the reuptake curves appear to be the most different between the curves, important information is garnered by comparing the entirety of the

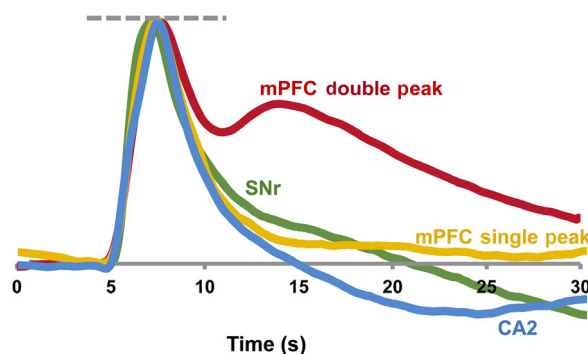


Fig. 8 The averages from each region have been normalized such that the maximum amplitude of each curve is at the horizontal blue dotted line. This allows for simple visual comparison of the reuptake curves.

reuptake profiles. Serotonin release in the CA2 appears primarily mediated by Uptake 2. The mPFC serotonin responses, as we previously characterized (West *et al.* 2018), involve clearance by both Uptake 1 and 2 transporters, which are linked inextricably to the two release domains. Serotonin released in the first domain, observed as a single peak, is reuptaken primarily by Uptake 2 mechanisms, whereas serotonin in the second domain is solely reuptaken by Uptake 1 processes. Domain 2 is only readily observed when measurements occur in layers 5–6 of the mPFC. In the SNr, serotonin seems to be reuptaken *via* a hybrid of Uptake 1 and 2.

These data lead us to formulate a hypothesis that the chemical decay profile after stimulation offered by the CFM is indicative of the ratio of SERT (Uptake 1) : non-SERT (Uptake 2) mediated serotonin reuptake. It follows that serotonin in the SNr and mPFC is more subject to Uptake 1 than serotonin in the CA2. It is important to note that in the mPFC, we measure as many single evoked events mediated by Uptake 2 (exclusively in layers 1–3) as we do double events (layers 5–6) incorporating both Uptake 1 and 2 (West *et al.* 2018). For this reason, we narrow down our postulate to serotonin in the SNr being cleared by a higher Uptake 1: Uptake 2 ratio when compared with the other two regions.

To strengthen this hypothesis, we perform ambient serotonin measurements with FSCAV in the three brain areas, shown in Fig. 4. In this study, we find that extracellular serotonin levels in the SNr are significantly lower than in the other two regions. This finding is in contrast to our early rationale, that because the SNr is highly innervated by serotonin fibers and this region contains a high tissue content of serotonin, that the SNr should contain a higher extracellular serotonin concentration.

We believe this low SNr basal level can also be explained by a higher ratio of SERT mediated reuptake in the SNr. At rest, ambient serotonin levels are primarily controlled by SERTs that are located, at high density, in the synaptic area (Zhou *et al.* 1998). However, because serotonin communication is characterized by volume transmission, this modulator can escape the synapse where it is more likely cleared by Uptake 2 mechanisms. Our electrical MFB stimulation is intense, with a high frequency and as such causes an atypically heavy efflux of serotonin, large enough to significantly escape the synapse. Thus, we observe Uptake 2 once the extracellular serotonin concentration is high enough to overcome a specific threshold. The stimulation allows us to test the local physiology of serotonin reuptake, yet the ambient level is more indicative of local SERT density (higher SERT density = lower extracellular serotonin).

This finding further supports our hypothesis that the SNr serotonin is reuptaken by a higher Uptake 1 : Uptake 2 ratio. To corroborate the rationale, we next turned to computational models to analyze the experimental data.

Mathematical modeling suggests physiological differences around CFM

We bring forth the idea that serotonin release in the SNr is reuptaken with a higher Uptake 1 : Uptake 2 ratio than in the CA2 or mPFC (*vide supra*). Here, we use previously established models to model experiment data and generate independent hypotheses (Fig. 5). As a reminder, the conclusions from the modeling are as follows:

- (i) Diffusion is needed to explain the double peaks seen in the PFC.
- (ii) There is a higher contribution of Uptake 1 in the SNr than in the other regions.
- (iii) The autoreceptor effect is strong in the SNr and CA2 but weak in the mPFC.
- (iv) The input strength to regions of the PFC is more variable than to the SNr and CA2.

Result (i) has already been validated and discussed in detail in prior work (West *et al.* 2018). Conclusion (ii) is in line with hypotheses brought forth from experimental data. The model has additionally suggested two more ideas in conclusions (iii) and (iv). We next further verify the Uptake 1 : Uptake 2 hypothesis and address these two novel concepts.

Verification of model hypotheses

The data and modeling thus far are highly interesting in that they imply that the voltammetric signal can provide information about local tissue physiology and the voltammetric circuitry. According to our model, the SNr evoked serotonin is subject to a higher ratio of Uptake 1 versus Uptake 2. It is not possible to say for certain, because the model reports a ratio, but this finding implies a higher density of SERTs in the SNr compared to the other regions. To address SERT density in each region, we first turned to the literature but were unable to find a single study that utilized a common technique to compare SERTs in the specific areas of all three regions we are interested in. Thus we employ a single-photon imaging approach, whereby axons are imaged in brain slices of adult serotonin transporter-EGFP BAC transgenic mice (Gong *et al.* 2003). It is well established that axonal innervation corresponds to SERT density (Jin *et al.* 2016). Images of axons and subsequent quantification of density (Fig. 6 and Table 1) illustrate a higher degree of serotonin axon innervation in the SNr compared to the two regions (innervation depends on layer and subregion of CA2 and mPFC). This is consistent with our model's hypothesis of higher ratio of Uptake 1–2 serotonin reuptake in the SNr. Thus these images provide support for the experimental and model Uptake 1 : Uptake 2 hypothesis.

We next explore an additional postulation offered by the model, that the excitation input to the mPFC is more variable than to the other two regions. While serotonin is elicited in all three regions *via* the common MFB stimulation, this does

not mean that the stimulation location is optimal for evoking maximal serotonin in all regions. If the stimulation location is optimal for eliciting maximal serotonin in all areas, systematically increasing the stimulation intensity, frequency and width should provide three serotonin profiles that plateau with the same characteristic. Thus, we perform experiments in five separate mice in each region whereby electrical stimulation frequency, amplitude, and pulse width are systematically altered. The standard stimulation utilized in our FSCV experiments is 120 pulses at 60Hz and 360 μ A, so the parameters are varied around this range Fig. 7 (top panel). The results from the stimulation paradigm study show that while the axons react in a similar manner to stimulation, the mPFC response does not plateau during any of the stimulation trains, whereas the CA2 and SNr responses clearly plateau during one or more of the experiments. This experiment shows that the stimulation location is less optimal for evoking maximal serotonin release in the mPFC, in accord with the model's postulate that the excitation input to the mPFC is more variable than to the other two regions.

An interesting side note is that a key difference between regions is observed during a depletion study where serotonin release is stimulated once a minute over a 20 min period in Fig. 7 (bottom panel). Here, only CA2 serotonin release is significantly depleted over 20 stimulations, whereas the SNr shows no depletion. A simplistic explanation for this difference is the tissue content differences between these regions, of which SNr contains much higher serotonin levels than the other regions (21.0 ± 1.6 ng/mg in the SNr vs. 0.98 ± 0.13 ng/mg in the hippocampus and 0.81 ± 0.065 ng/mg in the frontal cortex) (Shaskan and Snyder 1970; Kim *et al.* 2014). While it is worth noting that none of these experiments demonstrate the profound depletion that occurs in similar depletion studies with dopamine, this was previously attributed to the high cytosolic serotonin compared to the low amount released during each stimulation (Hashemi *et al.* 2012).

Thus, independently, two of the model's hypotheses are verified, again providing context that the chemical signals at the CFMs provide important information about localities and circuits. Another aspect of the model is to hypothesize that serotonin in the CA2 is more strongly autoregulated in comparison to the other two locals. It would be extremely challenging to independently verify this notion because of the large scope of serotonin autoreceptors and autoreceptor subtypes, and these autoreceptors' ability to synergize. However, the chemical signal and modeling that allude to autoreceptor control provide direction for future interest in autoreceptor-mediated serotonin regulation.

In sum, serotonin neurochemistry is important to study in the context of many brain disorders. FSCV and FSCAV are important tools to probe *in vivo* serotonin chemistry. In this paper, we compared two new voltammetric serotonin stimulation–measurement circuitries, in the CA2 region of the

hippocampus and the mPFC, to well-established SNr measurements. A common MFB stimulation evoked serotonin in all three brain localities where evoked and ambient serotonin were measured at the same electrode. We found differences in the serotonin chemistry between these three regions that we postulated to arise from differences in tissue physiology local to the CFM. By taking mathematical and imaging approaches, we validated this hypothesis. We therefore highlight the strength of fast voltammetric tools for providing physiological information that has implications for circuit mapping. A map of the circuits within specific brain regions ultimately allows for improved drug targeting for disease treatment.

Acknowledgments and conflicts of interest disclosure

This study was not pre-registered. This work was supported by the National Institutes of Health R01MH106563 (PH), P30GM103336-01A1 (EP), NS106491 and NS081467 (DJL), and Johns Hopkins Brain Science Institute grant (DJL). The authors declare no conflicts of interest for this work.

Open science badges

This article has received a badge for *Open Materials* because it provided all relevant information to reproduce the study in the manuscript. The complete Open Science Disclosure form for this article can be found at the end of the article. More information about the Open Practices badges can be found at <https://cos.io/our-service/s/open-science-badges/>

Supporting information

Additional supporting information may be found online in the Supporting Information section at the end of the article.

Data S1. Sample data used for preliminary power analysis calculation.

References

- Abdalla A., Atcherley C. W., Pathirathna P., Samaranyake S., Qiang B., Pena E., Morgan S. L., Heien M. L. and Hashemi P. (2017) In vivo ambient serotonin measurements at carbon-fiber microelectrodes. *Anal Chem* **89**, 9703–9711.
- Abi-Dargham A., Laruelle M., Aghajanian G. K., Charney D. and Krystal J. (1997) The role of serotonin in the pathophysiology and treatment of schizophrenia. *J. Neuropsychiatry Clin. Neurosci.* **9**, 1–17.
- Bremner J. D., Narayan M., Anderson E. R., Staib L. H., Miller H. L. and Charney D. S. (2000) Hippocampal volume reduction in major depression. *Am. J. Psychiatry* **157**, 115–118.
- Bremner J. D., Vythilingam M., Vermetten E., Nazeer A., Adil J., Khan S., Staib L. H. and Charney D. S. (2002) Reduced volume of orbitofrontal cortex in major depression. *Biol. Psychiatry* **51**, 273–279.
- Charan J. and Kantharia N. D. (2013) How to calculate sample size in animal studies? *J. Pharmacol. Pharmacother.* **4**, 303–306.
- Cohen J. (1988) *Statistical Power Analysis for the Behavioral Sciences*. Lawrence Erlbaum Associates, New York, NY.
- Franklin K. and Paxinos G. (2008) *The Mouse Brain in Stereotaxic Coordinates*. Academic Press, Cambridge, MA.
- Frodl T., Schaub A., Banac S., *et al.* (2006) Reduced hippocampal volume correlates with executive dysfunctioning in major depression. *J. Psychiatry Neurosci.* **31**, 316–323.
- Gina L., Andrew M., Jamie L. and Michael J. (2012) The role of the amygdala in anxiety disorders, in *The Amygdala* (Ferry B. ed.). IntechOpen, London.
- Gong S., Zheng C., Doughty M. L., *et al.* (2003) A gene expression atlas of the central nervous system based on bacterial artificial chromosomes. *Nature* **425**, 917–925.
- Gyorfi O., Nagy H., Bokor M., Moustafa A. A., Rosenzweig I., Kelemen O. and Keri S. (2017) Reduced CA2-CA3 hippocampal subfield volume is related to depression and normalized by 1-DOPA in newly diagnosed Parkinson's disease. *Front. Neurol.* **8**, 84.
- Hashemi P., Dankoski E. C., Petrovic J., Keithley R. B. and Wightman R. M. (2009) Voltammetric detection of 5-hydroxytryptamine release in the rat brain. *Anal. Chem.* **81**, 9462–9471.
- Hashemi P., Dankoski E. C., Lama R., Wood K. M., Takmakov P. and Wightman R. M. (2012) Brain dopamine and serotonin differ in regulation and its consequences. *Proc. Natl Acad. Sci. USA* **109**, 11510–11515.
- Jackson B. P., Dietz S. M. and Wightman R. M. (1995) Fast-scan cyclic voltammetry of 5-hydroxytryptamine. *Anal. Chem.* **67**, 1115–1120.
- Jin Y., Dougherty S. E., Wood K., *et al.* (2016) Regrowth of serotonin axons in the adult mouse brain following injury. *Neuron* **91**, 748–762.
- Johnson J. A., Rodeberg N. T. and Wightman R. M. (2018) Measurement of basal neurotransmitter levels using convolution-based nonfaradaic current removal. *Anal. Chem.* **90**, 7181–7189.
- Kim T. H., Choi J., Kim H. G. and Kim H. R. (2014) Quantification of neurotransmitters in mouse brain tissue by using liquid chromatography coupled electrospray tandem mass spectrometry. *J. Anal. Methods Chem.* **2014**, 506870.
- Kolb B., Mychasiuk R., Muhammad A., Li Y., Frost D. O. and Gibb R. (2012) Experience and the developing prefrontal cortex. *Proc. Natl Acad. Sci. USA* **109**(Suppl 2), 17186–17193.
- Lane R. and Baldwin D. (1997) Selective serotonin reuptake inhibitor-induced serotonin syndrome: review. *J. Clin. Psychopharmacol.* **17**, 208–221.
- Meunier C. J., Roberts J. G., McCarty G. S. and Sombers L. A. (2017) Background signal as an in situ predictor of dopamine oxidation potential: improving interpretation of fast-scan cyclic voltammetry data. *ACS Chem. Neurosci.* **8**, 411–419.
- Michael D. J., Joseph J. D., Kilpatrick M. R., Travis E. R. and Wightman R. M. (1999) Improving data acquisition for fast-scan cyclic voltammetry. *Anal. Chem.* **71**, 3941–3947.
- Muhammad A., Carroll C. and Kolb B. (2012) Stress during development alters dendritic morphology in the nucleus accumbens and prefrontal cortex. *Neuroscience* **216**, 103–109.
- Muller C. L., Anacker A. M. and Veenstra-VanderWeele J. (2016) The serotonin system in autism spectrum disorder: from biomarker to animal models. *Neuroscience* **321**, 24–41.
- Nestler E. J., Barrot M., DiLeone R. J., Eisch A. J., Gold S. J. and Monteggia L. M. (2002) Neurobiology of depression. *Neuron* **34**, 13–25.
- Oades R. D. (2008) Dopamine-serotonin interactions in attention-deficit hyperactivity disorder (ADHD). *Prog. Brain Res.* **172**, 543–565.
- Owens M. J. and Nemeroff C. B. (1994) Role of serotonin in the pathophysiology of depression: focus on the serotonin transporter. *Clin. Chem.* **40**, 288–295.
- Palkovits M., Brownstein M. and Saavedra J. M. (1974) Serotonin content of the brain stem nuclei in the rat. *Brain Res.* **80**, 237–249.
- Parsons L. H. and Justice J. B., Jr (1993) Serotonin and dopamine sensitization in the nucleus accumbens, ventral tegmental area, and

- dorsal raphe nucleus following repeated cocaine administration. *J. Neurochem.* **61**, 1611–1619.
- Rigucci S., Serafini G., Pompili M., Kotzalidis G. D. and Tatarelli R. (2010) Anatomical and functional correlates in major depressive disorder: the contribution of neuroimaging studies. *World J. Biol. Psychiatry* **11**, 165–180.
- Schumann C. M., Bauman M. D. and Amaral D. G. (2011) Abnormal structure or function of the amygdala is a common component of neurodevelopmental disorders. *Neuropsychologia* **49**, 745–759.
- Shaskan E. G. and Snyder S. H. (1970) Kinetics of serotonin accumulation into slices from rat brain: relationship to catecholamine uptake. *J. Pharmacol. Exp. Ther.* **175**, 404–418.
- Shen M., Qu Z., DesLaurier J., Welle T. M., Sweedler J. V. and Chen R. (2018) Single synaptic observation of cholinergic neurotransmission on living neurons: concentration and dynamics. *J. Am. Chem. Soc.* **140**, 7764–7768.
- Srejic L. R., Wood K. M., Zeqja A., Hashemi P. and Hutchison W. D. (2016) Modulation of serotonin dynamics in the dorsal raphe nucleus via high frequency medial prefrontal cortex stimulation. *Neurobiol. Dis.* **94**, 129–138.
- Uhlig C., Krause H., Koch T., de Abreu M. G. and Spieth P. M. (2015) Anesthesia and monitoring in small laboratory mammals used in anesthesiology, respiratory and critical care research: a systematic review on the current reporting in Top-10 impact factor ranked journals. *PLoS ONE* **10**.
- Volkow N. D. and Fowler J. S. (2000) Addiction, a disease of compulsion and drive: involvement of the orbitofrontal cortex. *Cereb. Cortex* **10**, 318–325.
- West A., Best J., Abdalla A., Nijhout F., Reed M. and Hashemi P. (2018) Voltammetric evidence for discrete serotonin circuits, linked to specific reuptake domains, in the mouse medial prefrontal cortex. *Neurochem. Int.* **123**, 50–58.
- Wood K. M., Zeqja A., Nijhout H. F., Reed M. C., Best J. and Hashemi P. (2014) Voltammetric and mathematical evidence for dual transport mediation of serotonin clearance in vivo. *J. Neurochem.* **130**, 351–359.
- Zhou F. C., Tao-Cheng J. H., Segu L., Patel T. and Wang Y. (1998) Serotonin transporters are located on the axons beyond the synaptic junctions: anatomical and functional evidence. *Brain Res.* **805**, 241–254.

Open Practices Disclosure

Manuscript Title: Fast Serotonin Voltammetry as a Versatile Tool for Mapping Dynamic Tissue Architecture: I. Responses at Carbon Fibers Describe Local Tissue Physiology

Corresponding Author: Parastoo Hashemi

Articles accepted to *Journal of Neurochemistry* after 01.2018 are eligible to earn badges that recognize open scientific practices: publicly available data, material, or preregistered research plans. Please read more about the badges in our *author guidelines and Open Science Badges page*, and you can also find information on the Open Science Framework [wiki](#).

Please check this box if you are interested in participating.

To apply for one or more badges acknowledging open practices, please check the box(es) corresponding to the desired badge(s) below and provide the information requested in the relevant sections. To qualify for a badge, you must provide a URL, doi, or other permanent path for accessing the specified information in a public, open-access repository. **Qualifying public, open-access repositories are committed to preserving data, materials, and/or registered analysis plans and keeping them publicly accessible via the web in perpetuity.** Examples include the Open Science Framework ([OSF](#)) and the various Dataverse networks. Hundreds of other qualifying data/materials repositories are listed at <http://re3data.org/>. Preregistration of an analysis plan must take place via a publicly accessible registry system (e.g., [OSF](#), [ClinicalTrials.gov](#) or other trial registries in the [WHO Registry Network](#), institutional registration systems). **Personal websites and most departmental websites do not qualify as repositories.**

Authors who wish to publicly post third-party material in their data, materials, or preregistration plan must have the proper authority or permission agreement in order to do so.

There are circumstances in which it is not possible or advisable to share any or all data, materials, or a research plan publicly. For example, there are cases in which sharing participants' data could violate confidentiality. If you would like your article to include an explanation of such circumstances and/or provide links to any data or materials you have made available—even if not under conditions eligible to earn a badge—you may write an alternative note that will be published in a note in the article. Please check this box if you would like your article to include an alternative note and provide the text of the note below:

Alternative note: The size and format of data files is incompatible with open sharing sites. The data is available upon request to the corresponding author.

Open Data Badge

1. Provide the URL, doi, or other **permanent path** for accessing the data in a **public, open-access repository**:

Confirm that there is sufficient information for an independent researcher to reproduce **all of the reported results**, including codebook if relevant.

Confirm that you have registered the uploaded files so that they are **time stamped** and cannot be age.

Open Materials Badge

1. Provide the URL, doi, or other **permanent path** for accessing the materials in a **public, open-access repository**: all relevant information is provided in the manuscript and custom-made materials will be provided upon reasonable request.

Confirm that there is sufficient information for an independent researcher to reproduce **all of the reported methodology**.

Confirm that you have registered the uploaded files so that they are **time stamped** and cannot be age.

Preregistered Badge

1. Provide the URL, doi, or other **permanent path** to the registration in a **public, open-access repository***:

2. Was the analysis plan registered prior to examination of the data or observing the outcomes? If no, explain.**

3. Were there additional registrations for the study other than the one reported? If yes, provide links and explain.*

*No badge will be awarded if (1) is not provided, **or** if (3) is answered “yes” without strong justification

**If the answer to (2) is “no,” the notation DE (Data Exist) will be added to the badge, indicating that registration postdates realization of the outcomes but predates analysis.

By signing below, authors affirm that the above information is accurate and complete, that any third-party material has been reproduced or otherwise made available only with the permission of the original author or copyright holder, and that publicly posted data do not contain information that would allow individuals to be identified without consent.

Date: 2/27/19

Name: Parastoo Hashemi

Signature: _____